Micro and Nano Systems Letters

CORRESPONDENCE Open Access

Surface roughness impact of 3D Ti-alloy printed WR-10 waveguide and rectangular horn antenna at W-band (75-110 GHz)

Cheolbok Kim[1], Ryan Cadwell[1], Anthony Ngoma[1], Zhong Yang[3], Md Mufassal Ahmad[2], Jungkwun Kim[2*] and Sung Jin Kim[3*]

Abstract

To investigate the effect of the surface roughness of 3D-metal-printed sub-THz components, the WR-10 3-inch-long waveguide and 24 dBi rectangular horn antenna were 3D-metal-printed using a titanium alloy powder and a high-resolution 3D metal printer. The characterized surface roughness of the printed components was 17.27 μm in RMS from a 3D optical surface profiler, and a nodule ratio of 7.89 μm and surface ratio of 1.52 for Huray model from the analyzed SEM images. The measured results of the 3D-metal-printed waveguide and rectangular horn antenna were compared with the ones of commercial waveguide and horn antenna having the same shapes. The 3D-metal-printed waveguide has 4.02 dB higher loss than the commercial waveguide, which may be caused by an ohmic loss of 0.85 dB and a surface roughness loss of 2.81 dB. The 3D-metal-printed horn antenna has 2 dB higher loss then the commercial horn antenna, which may be caused by an ohmic loss of 0.2 dB, surface roughness of 0.1 dB and fabrication tolerance loss of 1.7 dB. The loss separation was done from the EM simulation by changing the conductor material and surface roughness.

Introduction

For decades, 3D printing technology has been utilized to manufacture Radio Frequency (RF) components such as horn antennas, waveguides, and lenses, using a variety of technologies and materials [1–5] because it enables the prototype of a device quickly and to construct a complex 3D structure. In addition, 3D printing could be more cost-effective than traditional methods such as CNC and microfabrication. A range of 3D-printed RF components has been demonstrated across frequency bands from 20 to 400 GHz [6–11]. Among the various aspects of 3D-metal-printed structures, surface quality plays a critical role in determining electrical performance. This is particularly significant for high-frequency components, where a rough surface that exceeds the skin depth can lead to increased surface roughness losses. It is important to note that skin depth is inversely proportional to the square of the frequency. While several studies [1, 6, 9, 12] have assessed surface roughness in terms of Ra or RMS (root mean square), additional research may be needed to improve modeling accuracy. Furthermore, the effect of skin depth may differ depending on the type of RF component.

With the commercialization of 5G wireless communication systems operating at 28 GHz and 39 GHz, literature on 6G (sixth generation) wireless communication systems has begun to emerge [13]. Among the frequency ranges from 6 GHz to 1 THz, the 100 to

*Correspondence:
Jungkwun Kim
jungkwun.kim@unt.edu
Sung Jin Kim
sungjin.kim@louisville.edu
[1] Department of Research and Development, Corning Incorporated, Oneonta, NY 13820, USA
[2] Electrical Engineering, University of North Texas, Denton, TX 76203, USA
[3] Electrical and Computer Engineering, University of Louisville, Louisville, KY 40292, USA

200 GHz band is considered a strong candidate for 6G, as most of these bands are not yet allocated for specific applications [14, 15]. Therefore, there is an urgent need to develop RF components that operate between 100 and 200 GHz to support the demands of advanced wireless communication.

In this study, we fabricated two RF components—a WR-10 3-inch-long waveguide and a 24 dBi rectangular horn antenna—both operating in the W-band (75–110 GHz) using a titanium alloy (Ti-6Al-4 V Eli) and a high-resolution 3D metal printer. We evaluated the electrical performance of the printed waveguide and horn antenna with a Vector Network Analyzer (VNA) equipped with frequency extenders, and assessed the surface quality using a 3D optical surface profiler and a Scanning Electron Microscope (SEM). The performance of the 3D metal-printed components was compared with that of commercially available waveguides and horn antennas. Additionally, we used 3D electromagnetic (EM) simulations to investigate the sources of additional losses in the 3D metal-printed components. Using both empirical data and simulation, we investigated the minimum surface roughness needed to achieve performance comparable to that of commercially available RF components.

Design and fabrication

The WR-10 is a well-established standard for a rectangular waveguide at the W-band, covering the 75 to 110 GHz spectrum, with waveguide opening width and length of 2.54 mm and 1.27 mm, respectively. To investigate the effect of surface roughness on 3D metal-printed sub-THz RF components, we selected a 3-inch-long waveguide and a 24 dBi rectangular horn antenna which has an aperture size of 29.87×24.85 mm^2 and a length of 71.12 mm as test devices. and compared their performance with a commercial waveguide (SWG-10030-FB, Eravant) and a horn (SAR-2507-10-S2, Eravant) antenna of the same designs.

We fabricated the 3D metal-printed waveguide and horn antennas using a high-resolution metal 3D printer (3D Systems, ProX DMP 320) and fine powder of commercial Titanium alloy Grade 23 (Ti-6Al-4V ELI), an alpha–beta alloy containing 6% aluminium and 4% vanadium. During printing, argon gas was used in the chamber to prevent metal oxidation during the high-temperature process, which involved a 245 W high-power laser. We selected a resolution of 60 µm and a sidestep of 82 µm with extra-low interstitials for the waveguide and antenna structures. The 3D structure was formed by a laser in computer numerical control (CNC) mode, operating with a marked speed of 1250 mm/s.

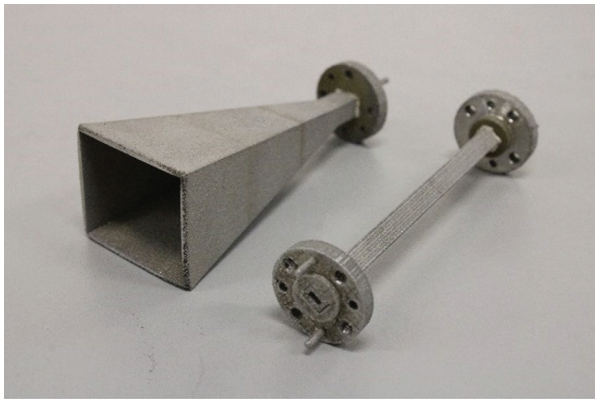

Fig. 1 Photo of the 3D-metal-printed WR-10 24dBi horn antenna (left) and 3-inch-long waveguide (right)

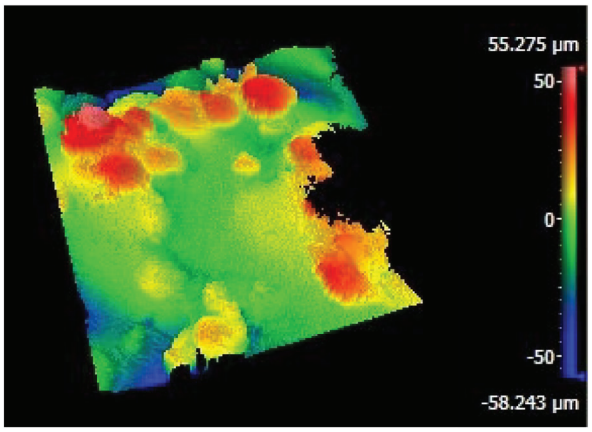

Fig. 2 3D optical surface image of the inside surface of the 3D-metal-printed horn antenna

Due to the complexity of the supporting materials and the deformation caused by internal stress during printing, we fabricated two separate parts (the WR-10 flange and the horn or waveguide) for assembly. After printing, the horn antenna and waveguide were assembled, and the WR-10 flange was soldered to the printed components using a conductive silver epoxy. Figure 1 shows the 3D metal-printed horn antenna and waveguide after the assembly process.

Analysis of surface roughness

The surface quality of the 3D-metal-printed horn and waveguide was characterized using Zygo's 3D optical surface profilometer and electron microscopes (SEM) images to include a surface roughness in the electromagnetic modeling. Figure 2 shows the surface image of the 3D-metal-printed structure using a 3D optical surface profiler. In the scanned 0.224×0.224 mm^2 area, the surface roughness of the printed structure was 13.76 µm in

Ra and 17.27 μm in RMS. *Ra* value was used as a simulation parameter for the Groisse model[16].

Figure 3a, b show the SEM images of the inside of the commercial horn and 3D-printed horn antennas, respectively. The surface of the commercial horn has only a small bump (top portion of particles) observed, while the surface of the 3D printed horn has several metal particles. Since the printing process was performed with fine powder, powder particles (also called nodules in the Huray model) were stuck on the surface of the melted titanium alloy, which caused the rough surface. The particle diameter and number were extracted from the SEM images using the MATLAB Image Processing Toolbox, as shown in Fig. 3, d.The commercial horn surface in Fig. 3a has 3138 particles in the area of 460×317 μm^2 and the average particle radius was 4.5 μm. One of the Huray model parameters, surface ratio (SR), was calculated by Eq. (1) [9], which is 1.12. Similarly, the 3D printed horn surface in Fig. 3b has 1303 particles In the area of 1130×780 μm^2, and the average particle radius was 11.79 μm. The calculated surface ratio (SR) is 2.58.

$$SR = \frac{4\pi r^2 N}{A} \tag{1}$$

where, N is the number of the particle, A is the area of the SEM image and r is the average radius of the particles.

Measurement

Both the 3-inch-long waveguide and the rectangular horn antenna were characterized using a Vector Network Analyzer (VNA), ZNC43, and W-band frequency upconverters, ZC110, from Rohde & Schwarz as shown in Fig. 4. The calibration for both measurements was done by the UOSM (Unknown through, Open, Shorn, Match) method. A measurement directly from the converter to the converter was carried out for the Unknown through, a short with a 90° shim offset was used for the Open, and the short and a matched termination were

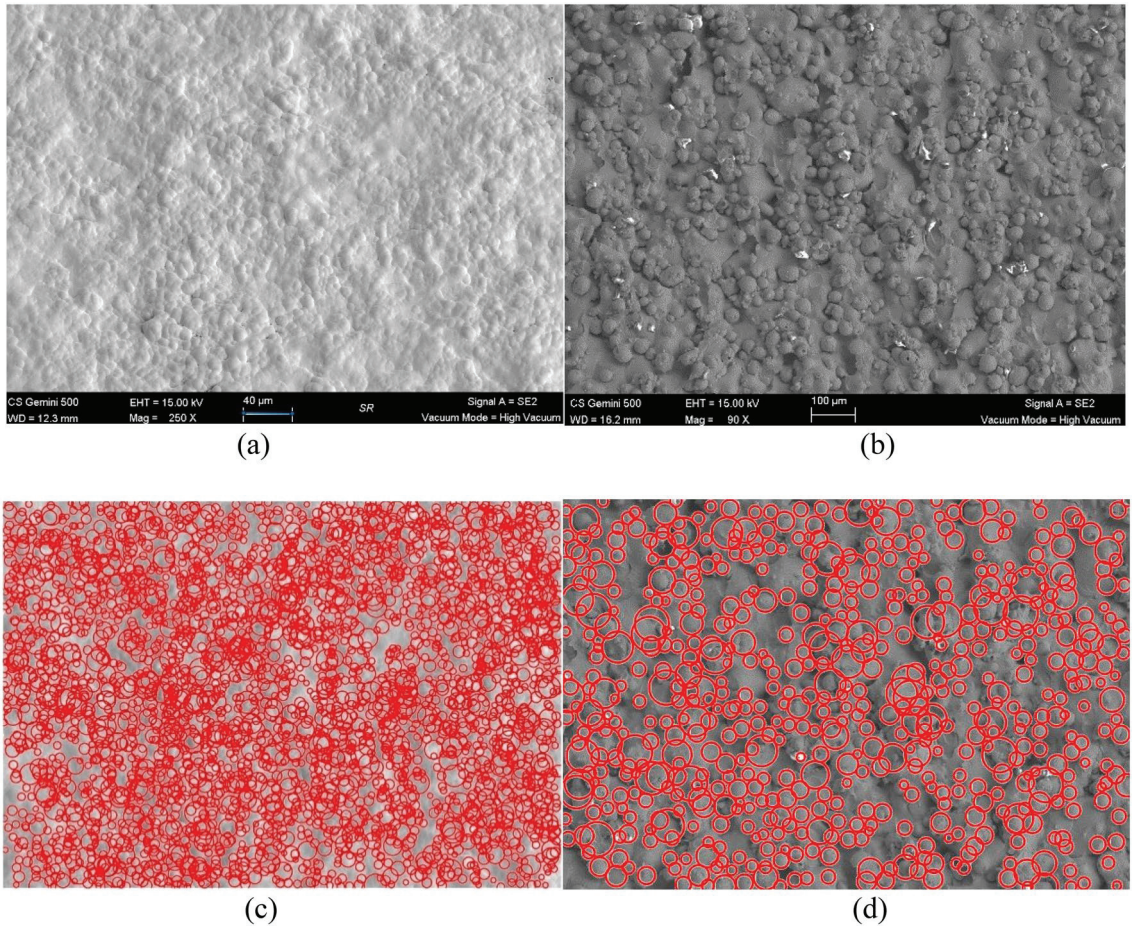

Fig. 3 SEM image of the horn antenna inside **a** commercial horn and **b** 3D metal printed horn. The analysis results of the SEM images: **c** commercial horn and **d** 3D printed horn to capture the number of titanium particles and their radius

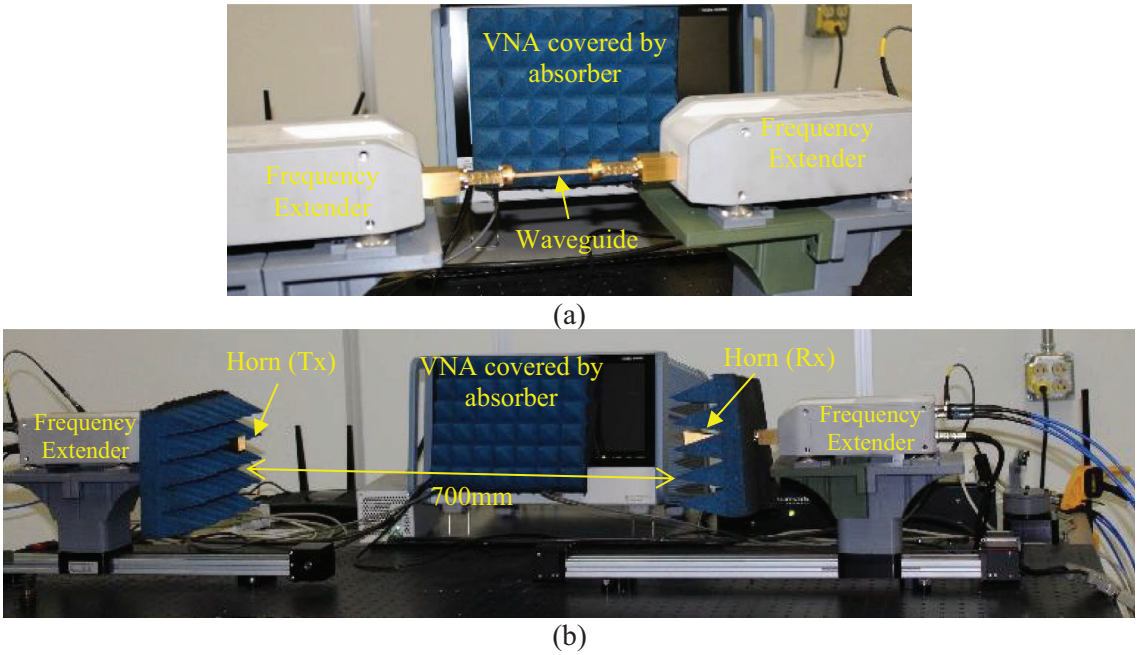

Fig. 4 Photos of the measurement setups: **a** waveguide and **b** horn antenna

used for the Short and Match. The measurement was performed by scanning the frequencies from 75 to 110 GHz with a step size of 0.35 GHz (101 points). The VNA's IFBW was set to 100 Hz for the measurement, and power at 0 dBm.

3-inch-long waveguide

After calibration of VNA with directly connected frequency extenders, the insertion loss of the 3-inch-long waveguides was measured by placing it between frequency extenders as shown in Fig. 4a. The return loss of the waveguides was measured by disconnecting the second converter and replacing it with the matched termination calibration standard.

24dBi rectangular horn antenna

The gain of the horn antenna was measured with a distance of 700 mm between the ends of the two horn antennas to ensure a far-field measurement as shown in Fig. 4b. First, we measured the insertion loss of two identical commercial horn antennas and calculated horn antenna gain by subtracting the path loss. Next, we replaced the receiver (Rx) horn with the 3D metal-printed horn to measure its gain. To eliminate undesired reflections from the signal of interest, we used a time gate function on the VNA with a time span of 600 ps and centered at 2.8 ps to minimize undesired reflection from the environment. For measuring the return loss, we removed the second antenna and replaced it with an absorber at the same distance. The return loss of the antenna was recorded without using a time gate, similar to the measurement method for waveguide return loss.

Results

Figure 5 shows the simulated and measured results of the 3-inch-long waveguides: commercial waveguide and 3D-metal-printed waveguide. The commercial waveguide was modelled with a smooth gold surface using a commercial 3D EM simulator, HFSS (High Frequency Structure Simulator) from Ansys. The 3D-metal-printed horn was modelled with three different conditions: (1) smooth titanium surface to get an ohmic loss only, (2) rough titanium surface with a Groisse model (Ra = 13.76 um), and (3) rough titanium surface with a Huray model (NR = 11.79 μm and SR = 2.58) [16].

Figure 5a shows the return losses of the simulated and measured waveguides. The waveguides show excellent impedance matching with a return loss of below − 20 dB. The measured 3D-metal-printed waveguide has a relatively worse return loss due to the rough surface of the waveguide flange. Figure 5b is the simulated and measured insertion losses. The simulated and measured insertion losses of the standard waveguide show a good agreement with the insertion loss of − 0.22 dB and − 0.28 dB at 100 GHz, respectively. The measured insertion loss of the 3D-metal-printed waveguide is − 4.02 dB at 100 GHz. The origins of the addition loss were investigated by modelling the antenna

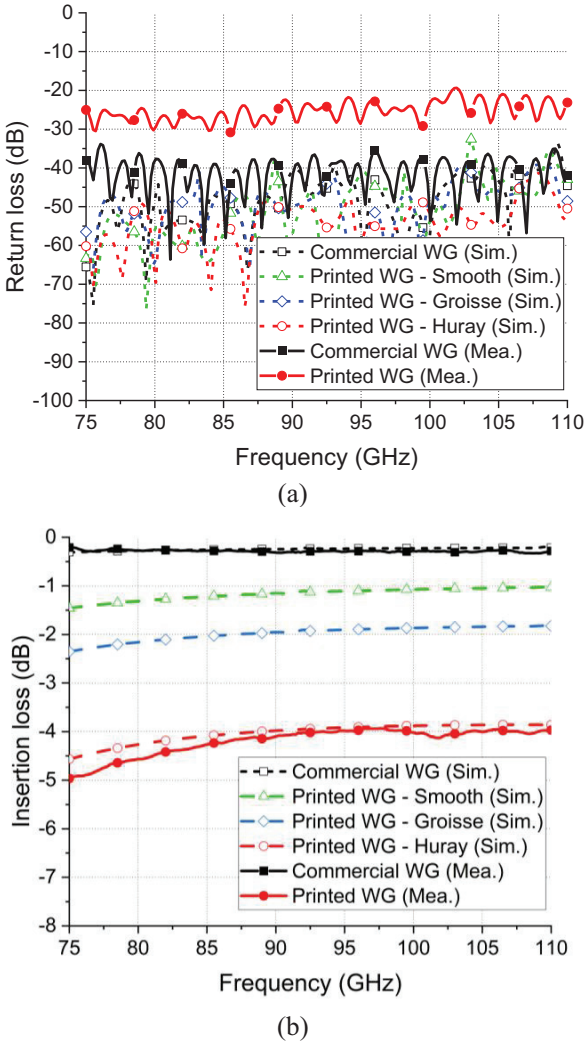

Fig. 5 Simulated and measured results of the 3-inch-long standard waveguide and 3D-metal-printed waveguide. **a** Return losses and **b** insertion losses

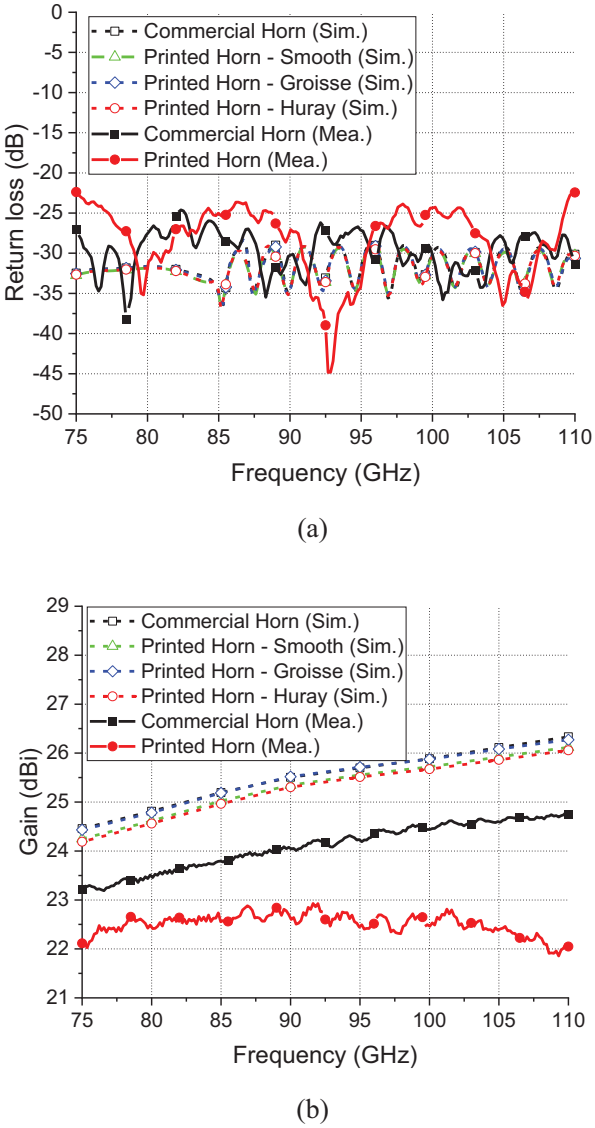

Fig. 6 Simulated and measured results of the standard 24 GHz horn antenna and 3D-metal-printed horn antenna. **a** Return losses and **b** gain

with different conductor materials and surface roughness. First, the identical waveguide structure was modelled with titanium instead of gold, which increased an insertion loss of − 1.07 dB. That means 0.85 dB loss comes from an Ohmic loss. We believe that the Ohmic loss is mostly related to its conductivity. The conductivity of titanium is 1.8×10^6 [S/m] which is 23 times lower than the one of gold, 4.1×10^7 [S/m]. Therefore, highly conductive metal for the 3D printed RF components is important to reduce their Ohmic losses. Next, the surface roughness loss was included in the modeling based on the Groisse model and Huray model although the accuracy of the models is not verified at W-band. The calculated insertion losses of the waveguide using Groisse and Huray models are − 1.86 dB and − 4.1 dB at 100 GHz, respectively. After considering the Ohmic loss value, we can identify the losses caused by the surface roughness as 0.7 dB with the Groisse model or 2.81 dB with the Huray model. The measured insertion loss of the 3D-metal-printed waveguide was well-matched with the simulated insertion loss including Ohmic loss and surface roughness loss along the frequency band.

Figure 6 shows the simulated and measured return losses and gains of the 24 dBi commercial rectangular horn and 3D-metal-printed rectangular horn at W-band. The simulated and measured horns show a good impedance matching with a return loss of below

– 20 dB as shown in Fig. 6a. Figure 6b shows the simulated and measured gain of the commercial and 3D-meatal printed rectangular horn antennas for comparison. In the simulation, the horn antenna gain was decreased 0.2 dB with Titanium from 25.9 dBi to 25.7 dBi at 100 GHz, which is ohmic loss. When the surface roughness was added in the modelling based on Huray model parameters, the horn antenna gain was 25.6 dBi, which is the surface roughness loss of 0.1 dB. In the measurement, the commercial horn antenna had a gain of 24.4 dBi at 100 GHz, while the 3D-metal-printed horn had a gain of 22.4 dBi, which is 2 dB lower than the one of the commercial horn. The 1.7 dB (=2 dB – 0.2 dB for ohmic loss—0.1dB for surface roughness loss) additional loss in measurement may be caused by the fabrication tolerance, especially the flatness of the flange.

Using both simulation and empirical data, we further investigated the component performance under different conditions of nodule size and surface ratio. Figure 7 illustrates the insertion loss values as a function of surface ratio and metal particle size. The lowest calculated insertion loss is −1.07 dB, primarily due to the low conductivity of titanium. This value could be significantly improved if the surface were plated with copper or silver. To achieve a minimum insertion loss of 2 dB as an example, a certain combination of the nodule radius and surface ratio is required. Thus, it is crucial to minimize the Ti-alloy particle size and employ advanced processing techniques to melt down all particles to achieve a smoother surface. Using Eq. 1, we can determine the required nodule radius to achieve the desired surface ratio.

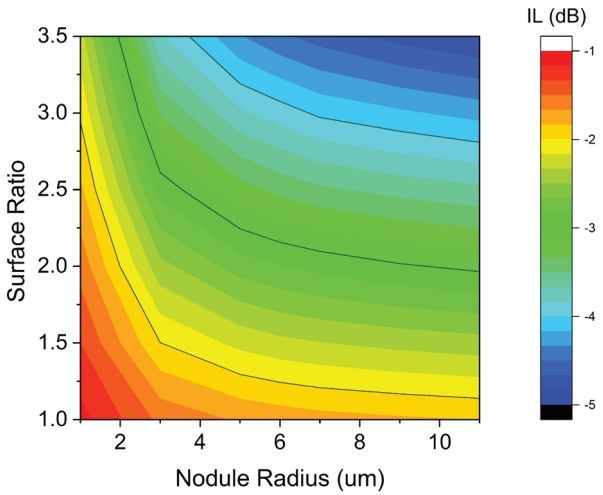

Fig. 7 The simulated insertion loss at 100 GHz with two different variables, surface roughness, and nodule radius. The maximum loss is 1.07 dB due to the conductor loss from the low conductivity of Ti alloy

Conclusion

The effect of surface roughness on 3D metal-printed RF components was investigated at W-band using a WR-10 3-inch-long waveguide and a 24 dBi rectangular horn antenna. These RF components were successfully fabricated using Titanium alloy Grade 23 and a high-resolution metal 3D printer. The 3D metal-printed waveguide and rectangular horn exhibited ohmic losses of 0.84 dB (~0.003 dB/mm) and 0.2 dB, respectively, and surface roughness losses of 2.81 dB (0.036 dB/mm) and 0.1 dB, respectively, at 100 GHz. The surface roughness loss was estimated by comparing the total loss of electromagnetic (EM) modeled total loss, including both ohmic and surface roughness losses based on characterized Huray model parameters, with the measured total loss. Simulation results indicate that reducing the Ti particle size is crucial for minimizing insertion loss. Additionally, employing a laser process to decrease the number of nodules would further improve the insertion loss.

Abbreviations

RF	Radio frequency
RMS	Root mean square
6G	Sixth generation
VNS	Vector network analyzer
SEM	Scanning electron microscope
EM	Electromagnetic
CNC	Computer numerical control
UOSM	Unknown through, Open, Shorn, Match
HFSS	High frequency structure simulator

Acknowledgements

The Authors would like to acknowledge Sarah E Roberts and Holly L Blodgett for surface quality characterization and Dr. Charles Tomonto, who assisted the metal 3D printing at the University of Miami.

Author contributions

Cheolbok Kim was responsible for RF characterization, surface analysis, and manuscript writing. Ryan Cadwell and Anthony Ngoma were responsible for RF measurement and SEM characterization. Md Mufassal Ahmad was responsible for the design and fabrication of the horn antenna and waveguide. Jungkwun Kim provided guidance throughout the design and fabrication processes of the antenna and waveguide and contributed to the preparation of the journal manuscript. Zhong Yang was responsible for 3D metal printing. Sung Jin Kim was responsible for designing the experiment for 3D metal printing and manuscript writing.

Funding

This work has been partially funded by the National Science Foundation (NSF) CNS 2039014, ECCS 2054567, ECCS 2029086, Korea Evaluation Institute of Industrial Technology (KEIT) 20018023, and NASA 80NSSC20K1204.

Data availability

All data generated or analyzed during this study are included in this submitted article. Data/Experimental results are presented in the manuscript and if appropriate, datasets/experimental results used and/or analyzed during the current study are available from the corresponding author on reasonable request.

Declarations

Competing interests
The authors declare no competing interests.

Received: 18 September 2024 Accepted: 11 December 2024
Published online: 19 December 2024

Publisher's Note

References

1. Zhang B, Guo YX, Zirath H, Zhang YP (2017) Investigation on 3-D-printing technologies for millimeter- wave and terahertz applications. Proc IEEE 105(4):723–736. https://doi.org/10.1109/JPROC.2016.2639520
2. Tan JY, Ciappesoni M, Kim SJ, Kim JJ (2021) Fabrication and characterization of titanium-alloy 3D printed solenoid inductors and their sensor applications. Eng Res Express 3(2):025031. https://doi.org/10.1088/2631-8695/ac008c
3. Gu C et al (2020) A D-Band 3D-Printed Antenna. IEEE Trans Terahertz Sci Technol 10(5):433–442. https://doi.org/10.1109/TTHZ.2020.2986650
4. Wang KX, Wong H (2017) A wideband millimeter-wave circularly polarized antenna with 3-D printed polarizer. IEEE Trans Antennas Propag 65(3):1038–1046. https://doi.org/10.1109/TAP.2016.2647693
5. Sage GPL (2016) 3D printed waveguide slot array antennas. IEEE Access 4:1258–1265. https://doi.org/10.1109/ACCESS.2016.2544278
6. Fiorese V et al. Evaluation of micro laser sintering metal 3d-printing technology for the development of waveguide passive devices up to 325 GHz. In: 2020 IEEE/MTT-S International Microwave Symposium (IMS), 4–6 Aug 2020. 2020, pp. 1168–1171. https://doi.org/10.1109/IMS30576.2020.9224102.
7. Shah SDA, Li H, Kuhlmey B, Atakaramians S, 3D printed horn coupler for hybrid photonic crystal THz waveguides. In: 2021 46th International Conference on Infrared, Millimeter and Terahertz Waves (IRMMW-THz), 29 Aug.-3 Sept 2021. 2021, pp. 1–2, https://doi.org/10.1109/IRMMW-THz50926.2021.9567582.
8. Standaert A, Reynaert P, A 400 GHz Transmitter integrated with flip-chiped 3D printed horn antenna with an EIRP of 1.26dBm. In: 2018 IEEE/MTT-S International Microwave Symposium - IMS, 10–15 June 2018 2018, pp. 141–144. https://doi.org/10.1109/MWSYM.2018.8439273.
9. Sun F, Li Y, Wang J. 3D Printed 60-GHz High-Gain Horn Antenna Arrays with 40% Bandwidth. In: 2020 IEEE Asia-Pacific Microwave Conference (APMC), 8–11 Dec. 2020 2020, pp. 480–482, https://doi.org/10.1109/APMC47863.2020.9331604.
10. Zhang B et al (2016) Metallic 3-D printed antennas for millimeter- and submillimeter wave applications. IEEE Trans Terahertz Sci Technol 6(4):592–600. https://doi.org/10.1109/TTHZ.2016.2562508
11. Zhang B, Zirath H (2016) Metallic 3-D printed rectangular waveguides for millimeter-wave applications. IEEE Trans Comp Pack Manuf Technol 6(5):796–804. https://doi.org/10.1109/TCPMT.2016.2550483
12. Almeshehe M et al (2022) Surface roughness impact on the performance of the 3D metal printed waveguide coupler at millimeterwave band. Eng Sci Technol Int J 35:101129. https://doi.org/10.1016/j.jestch.2022.101129
13. Tataria H, Shafi M, Molisch AF, Dohler M, Sjöland H, Tufvesson F (2021) 6G wireless systems: vision, requirements, challenges, insights, and opportunities. Proc IEEE 109(7):1166–1199. https://doi.org/10.1109/JPROC.2021.3061701
14. Farid AA, Ahmed ASH, Dhananjay A, Rodwell MJW (2022) A fully packaged 135-GHz multiuser MIMO transmitter array tile for wireless communications. IEEE Trans Microw Theory Tech 70(7):3396–3405. https://doi.org/10.1109/TMTT.2022.3161972
15. Rappaport TS et al (2019) Wireless communications and applications above 100 GHz: opportunities and challenges for 6G and beyond. IEEE Access 7:78729–78757. https://doi.org/10.1109/ACCESS.2019.2921522
16. Griesi MB. Characterization of electrodeposited copper foil surface roughness for accurate conductor power loss modelling. Univ. of South Carolina,, vol. Thesis, 2014.